Biochimica et Biophysica Acta 1787 (2009) 955–962

Contents lists available at ScienceDirect

Biochimica et Biophysica Acta

journal homepage: www.elsevier.com/locate/bbabio

On chemomechanical coupling of the F_1-ATPase molecular motor

Ping Xie

Laboratory of Soft Matter Physics, Institute of Physics, Chinese Academy of Sciences, Beijing 100190, China

ARTICLE INFO

Article history:
Received 27 November 2008
Received in revised form 19 February 2009
Accepted 19 February 2009
Available online 2 March 2009

Keywords:
F_1-ATPase
Mechanochemical coupling mechanism
Rotary molecular motor
Hexameric motor protein

ABSTRACT

F_1-ATPase catalyzes ATP hydrolysis to drive the central γ-shaft rotating inside a hexameric cylinder composed of alternating α and β subunits. Experiments showed that the rotation of γ-shaft proceeds in steps of 120° and each 120°-rotation is composed of an 80° substep and a 40° substep. Here, based on the previously proposed models, an improved physical model for chemomechanical coupling of F_1-ATPase is presented, with which the two-substep rotation is well explained. One substep is driven by the power stroke upon ATP binding, while the other one resulted from the passage of γ-shaft from previous to next adjacent β subunits via free diffusion. Using the model, the dynamics and kinetics of F_1-ATPase, such as the rotating time of each substep, the dwell time at each pause and the rotation rate, are analytically studied. The theoretical results obtained with only three adjustable parameters reproduce the available experimental data well.

1. Introduction

ATP synthase is a universal enzyme that uses the proton-motive force across the mitochondrial membranes to make ATP from ADP and Pi [1–3]. It consists of two portions Fo and F_1 connected to a common shaft — the γ-shaft. Under normal circumstances, the transmembrane portion Fo drives the rotation of the γ-shaft to release newly synthesized ATP from the globular catalytic moiety F_1. The F_1 portion has three α and three β subunits arranged in alternation around the γ-shaft. All of α and β subunits can bind nucleotide, but only the three β subunits are catalytic active.

When the F1 portion is not coupled to the Fo portion, it can work in the opposite direction hydrolyzing ATP and driving the rotation of the γ-shaft, as a molecular motor called F_1-ATPase. Rotation of the γ-shaft in F_1-ATPase has been demonstrated experimentally by various methods [4,5]. In particular, by attaching a fluorescent actin filament to the γ-shaft, the rotation with discrete 120° steps has been observed directly [6,7]. Later experiments reduced the frictional drag on the rotation by using a colloidal bead attached to the γ-shaft [8]. The experiments revealed that each 120° rotation is resolved into a 90° substep and a 30° substep. The 90° and 30° substeps were recently revised to be 80° and 40° substeps, respectively [9,10]. The pause at $\theta = 0°$ is dependent on ATP concentration while the pause at $\theta = 80°$ is ATP-concentration independent.

From theoretical point of view, several insightful models and various mathematical approaches have been proposed for the chemomechanics of F_1-ATPase motor [11–18]. The model of Wang and Oster [11] provides a physical answer to the rotational dynamics of F_1-ATPase — the hinge-bending motion of β subunit induced by ATP binding drives the eccentric γ-shaft rotating 120° during an ATPase cycle. With this model, numerical studies of kinetics and dynamics of F_1-ATPase based on a set of complicated coupled Fokker–Planck equations have been presented [11]. Recently, Gaspard and Gerritsma [12] have also given the numerical studies based on a set of simplified coupled Fokker–Planck equations. The experimentally observed two substeps in a 120° rotation have been explained physically as follows [13]. The pause at $\theta = 0°$ is due to waiting for ATP binding to subunit 1 (defined in Fig. 5d of Sun et al. [13]). Some of the free energy induced by the ATP binding in site 1 drives the rotation of first substep. The pause at $\theta = 80°$ is due to the hindering of subunit 3 bound with ADP. After the ADP in subunit 3 is released, the remaining free energy induced by the ATP binding in site 1 completes the second substep. On the other hand, various other models focused on the kinetics and/or dynamics of F_1-ATPase have been presented by other researchers [14–18]. With these models, simple and analytical formulae have been derived, thus giving more explicit descriptions of the rotational behaviors.

In this work, on the basis of the previous models [11–13,16], an improved model is presented for the chemomechanical coupling of the F_1-ATPase molecular motor. The present model gives naturally that each 120° rotation of the γ-shaft is composed of two substeps. The first substep of 80° rotation is driven by hinge-bending motion of β subunit; while the second substep of 40° rotation is due to the passage of the γ-shaft from previous to next adjacent β subunits. With the model, the rotation rates of the motor under different values of viscous friction and ATP concentration are analytically studied, giving the results similar to those obtained from previous models [11–13,16]. Moreover, the mean rotating time of each substep and the dwell-time distribution at each pause are analytically studied. All the theoretical results reproduce the available experimental data well.

E-mail address: pxie@aphy.iphy.ac.cn.

0005-2728/$ – see front matter © 2009 Elsevier B.V. All rights reserved.
doi:10.1016/j.bbabio.2009.02.017

2. Model

Before the presentation of the model for chemomechanical coupling of F_1-ATPase molecular motor, three preliminary hypotheses are presented as follows.

(1) The strength of γ-shaft interacting with a β subunit depends on the nucleotide state of the β subunit. In nucleotide free, ATP and ADP.Pi states the β subunit has a strong interaction with γ-shaft; while in the ADP state the β subunit has a weak interaction with γ-shaft. This assumption can be understood as follows. The nucleotide transition induces the conformational change on the interaction region of the β subunit with γ-shaft. This induces the change of negative charge distributions on the interaction region of the β subunit, thus resulting in the change of the electrostatic interaction between the β subunit and γ-shaft [19]. The assumption is also based on the analogy to other ring-shaped hexameric nucleic-acid motor proteins that have similar structures to the F_1-ATPase. For example, the hexameric nucleic-acid motor proteins such as bacteriophage T7 DNA helicase [20], RuvB [21] and ϕ29 DNA packaging motor [22] have been shown experimentally to have nucleotide-dependent affinities for DNA. In fact, it seems a universal property that a molecular motor capable of converting chemical energy of ATP hydrolysis into mechanical energy shows nucleotide-dependent affinities for its track (e.g., kinesin for microtubule; myosin for actin; T7 DNA helicase, RuvB and ϕ29 DNA packaging motor for DNA; β subunits for γ-shaft in F_1-ATPase).

(2) The strong interaction of γ-shaft interacting with a β subunit stimulates significantly the ATP-binding rate, ATP-hydrolysis rate and Pi-release rate of the β subunit. This assumption is similar to that adopted by Oster et al. [11,13] and is supported by the following experimental evidences. Mutation studies of amino acid residues along the γ-shaft have identified several critical positions [23,24]. Substitution of these critical amino acids results in a dramatic reduction in the overall hydrolysis rate. Examining the sequence of interpolated structures reveals that these critical residues make contact with two regions on the β subunit. The first region is the helix–turn–helix (HTH) domain at the C-terminal end of the β subunit; this is the place where the β subunit interacts with the γ-shaft. Clearly, disturbing this region affects the power-stroke motion. The second region is another HTH domain directly behind the ATP-binding pocket. Both of these HTH domains lie within loops emanating from the same β-sheet whose loops grasp the nucleotide [13]. Thus, chemical transitions in the binding pocket are directly coupled to the interaction with the γ-shaft.

(3) As shown structurally [25], ATP binding induces the β subunit to bend from open to close conformations; while the release of ADP induces the β subunit to return from close to open conformations. Furthermore, it is shown from the structure [25] that the bending motion of the β subunit driven by ATP binding pushes against the eccentric γ-shaft rotated by about 80° in the counterclockwise direction (see from the top). Since this bending motion drives the rotation of γ-shaft, it is also called power-stroke motion.

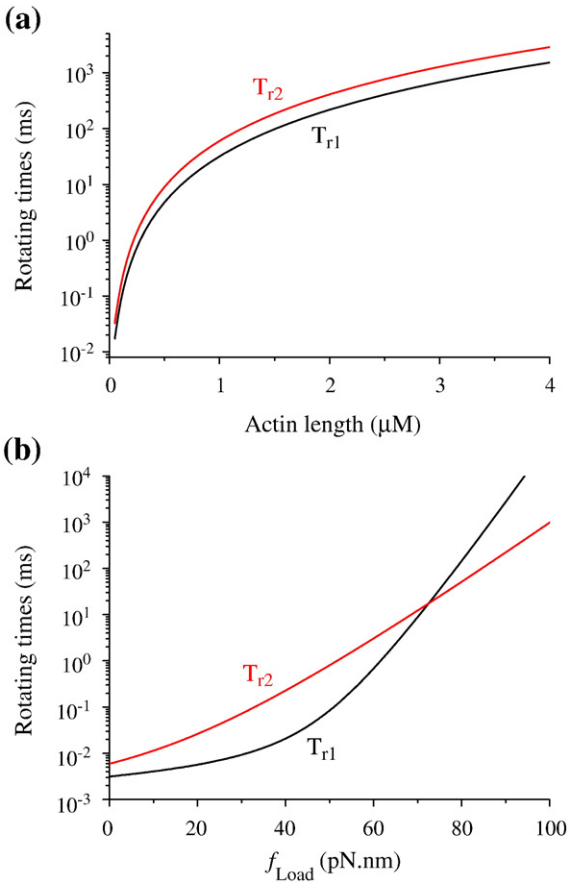

Fig. 2. Rotating time T_{r1} from 0 to 80° and rotating time T_{r2} from 80° to 120°. (a) T_{r1} and T_{r2} as a function of the length of actin filament in the case of $f_{Load} = 0$. (b) T_{r1} and T_{r2} as a function of f_{Load} without actin filament attached to the γ-shaft.

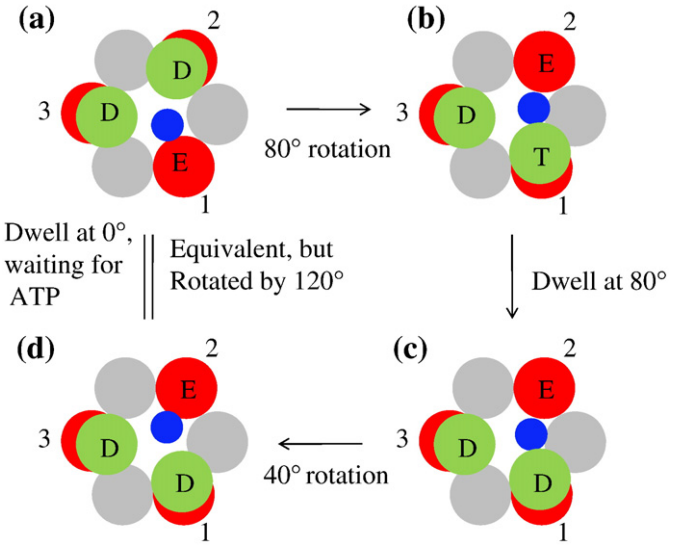

Fig. 1. Schematic illustrations of chemomechanics by F_1-ATPase. The γ-shaft is drawn in blue, the α subunit in grey, the open β subunit in red, the upper potion of closed β subunit in green and the lower portion of closed β subunit in red. (a) β subunit 1 in nucleotide free state binds the γ-shaft. β subunit 2 is bound with ADP and β subunit 3 is bound with ADP. (b) Upon ATP binding, the bending motion of β subunit 1 pushes the eccentric γ-shaft rotating by 80°. ADP is released from β subunit 2. (c) After ATP hydrolyzes to ADP.Pi and then Pi is released, β subunit 1 in ADP state becomes weakly interacting with the γ-shaft. (d) Since now β subunit 1 in ADP state has a weak interaction with the γ-shaft while nucleotide free β subunit 2 has a strong interaction with the γ-shaft, the γ-shaft is detached from subunit 1 and binds subunit 2 via a 40° rotation.

Based on above hypotheses, we propose the model, which is schematically illustrated in Fig. 1. We begin with β subunit 1 in nucleotide free state binding the γ-shaft. Now β subunit 2 is either bound with ADP or nucleotide free and β subunit 3 is bound with ADP (Fig. 1a) (see discussion on sequential ATPase activities in Section 6.1). Stimulated by the interaction with the γ-shaft, β subunit 1 binds ATP with a high rate. Upon ATP binding, the bending motion of β subunit 1

pushes the eccentric γ-shaft rotating by 80° (Fig. 1b). Then ATP hydrolyzes to ADP.Pi. After Pi is released, β subunit 1 in ADP state becomes weakly interacting with the γ-shaft (Fig. 1c). Note that, during the period of ATP binding, ATP hydrolysis and Pi release in subunit 1, ADP has been released from subunit 2 if $2(k_2^{-1}+k_3^{-1})>k_4^{-1}$, where k_2 and k_3 are the ATP-hydrolysis rate and Pi-release rate, respectively, of the β subunit that binds the γ-shaft and k_4 is the ADP-release rate. Since now β subunit 1 in ADP state has a weak interaction with the γ-shaft while nucleotide free β subunit 2 has a strong interaction with the γ-shaft, the γ-shaft is detached from subunit 1 and binds subunit 2 via a 40° rotation (Fig. 1d). Fig. 1d is the same as Fig. 1a except that the γ-shaft is rotated by 120° and the F_1-ATPase hydrolyzes an ATP. Then the next mechanical step coupled with hydrolysis of another ATP proceeds.

In this model, there exist two substeps in a rotation of 120°, with the first substep from 0 to 80° and the second substep from 80° to 120°. The first substep immediately follows the ATP binding. During this first substep, an intrinsic driving torque is present, which resulted from the bending motion of the β subunit (or the power-stroke motion) driven by ATP binding, and the rotation is mainly driven by the driving torque. The second substep immediately follows (or is related to) the release of Pi, which is consistent with the recent experimental results of Adachi et al. [26]. As structure shows, the β subunit in ATP, ADP.Pi and ADP states has the same close conformation [25], implying that no power stroke occurs related to Pi release. Thus, during the second substep, no intrinsic driving torque is present and the rotation resulted from the free diffusion due to the thermal noise. Note that the occupancy state in Fig. 1b (with subunit 1 bound with ATP, subunit 2 with no nucleotide and subunit 3 bound with ADP) corresponds to F_1-ATPase structure originally observed by Abrahams et al. [25]. This represents the catalytic dwell state before the second substep, which is consistent with the experimental results [27]. Note also that the β subunit 1 to which an ATP binds is not the one (β subunit 2) from which ADP is released (see Figs. 1a and b), which is consistent with the recent experimental results of Adachi et al. [26].

3. Rotating times

Similar to that presented in previous works [11–13,16], the rotation of γ-shaft can be quantitatively described by the following Langevin equation

$$\zeta\frac{d\theta}{dt}=f_{\mathrm{Drive}}-f_{\mathrm{Load}}+f_{\mathrm{B}}(t), \tag{1}$$

where θ is the rotational angle of the γ-shaft; ζ is the drag coefficient against the rotation; f_{Drive} is the intrinsic driving torque that resulted from the bending motion of the β subunit driven by ATP binding during the first substep, while $f_{\mathrm{Drive}}=0$ during the second substep; f_{Load} is the torque resulted from an external force (e.g., a magnetic trap); and $f_{\mathrm{B}}(t)$ is the Brownian torque due to the thermal noise. It is

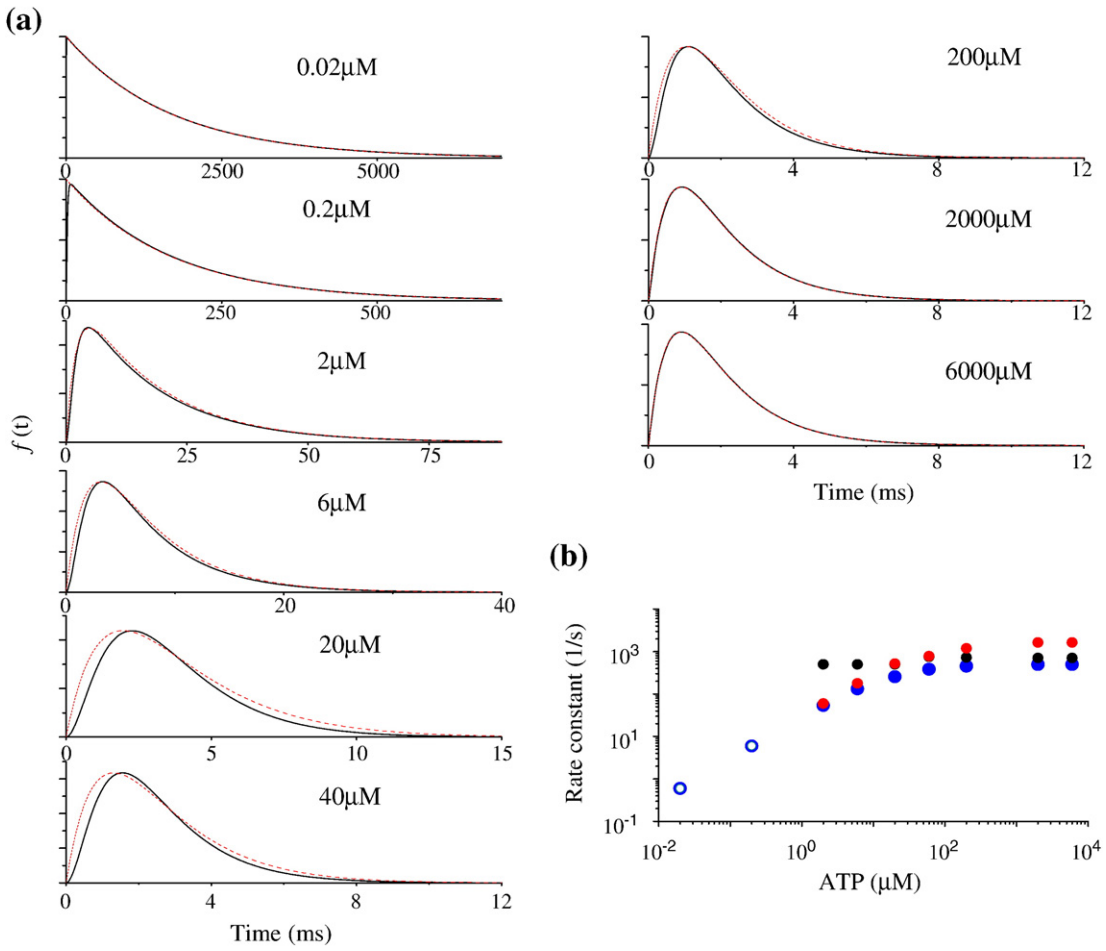

Fig. 3. Dwell-time distributions. (a) Dwell-time distributions calculated by using Eq. (9) at different ATP concentrations (black solid lines). Red dashed lines at 0.02 and 0.2 μM are calculated by using $f(t)=k_1\exp(-k_1t)$, with $k_1=k_b$[ATP] (open circles in b). Red dashed lines at 2, 6, 20, 60 and 200 μM are two-exponential fits to the black solid lines, constant × [exp $(-k_{a1}t)-\exp(-k_{a2}t)$], with k_{a1} and k_{a2} shown (filled black and red circles in b). Red dashed lines at 2000 and 6000μM are calculated by using $f(t)=k_2k_3/(k_2-k_3)$ [$\exp(-k_2t)-\exp(-k_3t)$], with k_2 and k_3 shown (filled black and red circles in b). (b) ATP dependence of the rate constants. Blue circles show the total rates k_1 or $k_{a1}k_{a2}/(k_{a1}+k_{a2})$ or $k_2k_3/(k_2+k_3)$.

noted here that the drag friction, which is contained in the drag coefficient ζ, is composed of both the friction against the rotation without external load acting on the γ-shaft and the friction due to the external load (e.g., due to an actin filament or a bead attached to the γ-shaft). The external torque f_{Load} represents only the torque that resulted from the external force; whereas the drag friction induced by the external load is not contained in f_{Load} but is contained in ζ.

The magnitude of f_{Drive} can be obtained from the free energy computed from the uni-site kinetics [28,29]. Of the total free-energy drop of about $24k_{\mathrm{B}}T$ for the hydrolysis of an ATP molecule, there are two free-energy drops: $14k_{\mathrm{B}}T$ upon ATP binding and $10k_{\mathrm{B}}T$ upon product release. The first drop is attributed to the bending motion of the β subunit from open to close conformations driven by ATP binding, while the second drop to the returned unbending motion of the β subunit to its open conformation. Since only the ATP binding induces the power stroke via the bending motion of the β subunit to its close conformations, the driving torque should be calculated using the first free-energy drop. Moreover, bending of the β subunit is driven by the progressive annealing of hydrogen bonds between ATP and the catalytic site, which generates a nearly constant bending torque on the β subunit [11,13]. Thus, the driving torque can be calculated by $f_{\mathrm{Drive}}=14k_{\mathrm{B}}T\times 9/(4\pi)$. The drag coefficient is calculated by $\zeta=\zeta_0+\zeta_{\mathrm{Ext}}$, where $\zeta_0=10^{-4}$ pN nm s is the drag coefficient against the rotation without external load acting on the γ-shaft and ζ_{Ext} is the drag coefficient due to the external load. In the case of F_1-ATPase driving an actin filament, $\zeta_{\mathrm{Ext}}=\frac{4\pi}{3}\eta L^3/[\ln(L/2r)-0.447]$ [30,31], where $\eta=0.01$ g cm^{-1} s^{-1} is the viscosity of the aqueous medium, L is the length of actin filament and $r=5$ nm is the radius of the filament. In the case of fluorescent beads, $\zeta_{\mathrm{Ext}}=10.5\pi\eta R_{\mathrm{B}}^3$ [13], where R_{B} is the radius of the bead. The Brownian torque in Eq. (1) satisfies $\langle f_{\mathrm{B}}(t)\rangle=0$ and $\langle f_{\mathrm{B}}(t)f_{\mathrm{B}}(t')\rangle=2k_{\mathrm{B}}T\zeta\delta(t-t')$.

From Eq. (1) the mean first-passage time for the γ-shaft to rotate an angle of Θ is obtained as follows [32]

$$T_{\mathrm{r}}=\frac{1}{A}\left\{\frac{D}{A}\left[\exp\left(-\frac{A}{D}\Theta\right)-1\right]+\Theta\right\}, \tag{2}$$

where $A\equiv(f_{\mathrm{Drive}}-f_{\mathrm{Load}})/\zeta$ and $D\equiv k_{\mathrm{B}}T/\zeta$. In the case of external torque $f_{\mathrm{Load}}=0$, from Eq. (2), the mean rotating time of the first substep is

$$T_{\mathrm{r1}}=\frac{\zeta}{f_{\mathrm{Drive}}}\left\{\frac{k_{\mathrm{B}}T}{f_{\mathrm{Drive}}}\left[\exp\left(-\frac{f_{\mathrm{Drive}}}{k_{\mathrm{B}}T}\cdot\frac{4\pi}{9}\right)-1\right]+\frac{4\pi}{9}\right\}, \tag{3}$$

and the mean rotating time of the second substep is

$$T_{\mathrm{r2}}=\left(\frac{2\pi}{9}\right)^2\zeta/(2k_{\mathrm{B}}T). \tag{4}$$

Using Eqs. (3) and (4) the calculated results of T_{r1} and T_{r2} as a function of the length of actin filament attached to the γ-shaft are shown in Fig. 2a. Although the first substep has a step size of 2 folds of that of the second substep, the rotating time of the first substep is shorter than that of the second substep. This is because the rotation in the first substep is driven by the bending motion of the β subunit while the rotation in the second substep is due to the free diffusion. As actin length increases, both rotating times T_{r1} and T_{r2} increase significantly. As we will see below (Fig. 4), these significant increases of T_{r1} and T_{r2} with actin length reduce the rotation rate.

Using Eq. (2) the calculated results of T_{r1} and T_{r2} as a function of f_{Load} without actin filament attached to the γ-shaft are shown in Fig. 2b. It is seen that, for an external torque $f_{\mathrm{Load}}\leq 40$ pN nm, the total rotating time $T_{\mathrm{r1}}+T_{\mathrm{r2}}<0.25$ ms, which is much shorter than the dwell time even at saturating ATP concentration (2.3 ms) (see below). For $f_{\mathrm{Load}}<72.5$ pN nm, the rotating time of the first substep is shorter than that of the second substep; while for $f_{\mathrm{Load}}>72.5$ pN nm the rotating time of the first substep becomes longer than that of the second substep. By comparing Fig. 2a with Fig. 2b, it is noted that an external torque of as large as 91 pN nm results in about a same reduction of rotating time as that of an actin with length of 4 μm.

4. Dwell times

First, we study the 0° dwell time. The 0° dwell period corresponds to the scheme, Empty $\xrightarrow{k_1}$ ATP, where $k_1=k_{\mathrm{b}}[\mathrm{ATP}]$ is approximately the ATP-binding rate of the β subunit that binds the γ-shaft, because the ATP-binding rate of the β subunit without interaction with the γ-shaft is negligibly small. From this scheme, we can easily obtain that the mean 0° dwell time is

$$T_{\mathrm{d1}}=\frac{1}{k_{\mathrm{b}}[\mathrm{ATP}]}. \tag{5}$$

This implies that the mean 0°dwell time is inverse proportional to ATP concentration.

Second, we study the 80°dwell time. Here it is considered that $2(k_2^{-1}+k_3^{-1})>k_4^{-1}$. Thus, the 80°dwell period corresponds to the scheme, ATP $\xrightarrow{k_2}$ ADP.Pi $\xrightarrow{k_3}$ ADP. From this scheme, the mean 80°dwell time is obtained as follows

$$T_{\mathrm{d2}}=\frac{k_2+k_3}{k_2k_3}. \tag{6}$$

This implies that the mean 80°dwell time is independent of ATP concentration.

Third, we study the dwell time between two main steps, as measured in Yasuda et al. [8]. This period corresponds approximately to the following scheme for the β subunit that binds the γ-shaft:

$$\mathrm{Empty}\xrightarrow{k_1}\mathrm{ATP}\xrightarrow{k_2}\mathrm{ADP.Pi}\xrightarrow{k_3}\mathrm{ADP}. \tag{7}$$

In the following, we denote the probabilities for finding the β subunit in Empty (nucleotide free), ATP, ADP.Pi and ADP states by ϕ, T, DP, and D respectively. From Eq. (7), the probabilities are described by the following differential equations

$$\frac{\mathrm{d}\phi}{\mathrm{d}t}=-k_1\phi, \tag{8a}$$

$$\frac{\mathrm{d}T}{\mathrm{d}t}=k_1\phi-k_2T, \tag{8b}$$

$$\frac{\mathrm{d}(DP)}{\mathrm{d}t}=k_2T-k_3(DP), \tag{8c}$$

$$\frac{\mathrm{d}D}{\mathrm{d}t}=k_3(DP). \tag{8d}$$

By solving Eqs. (8a)–(8d), with the initial conditions at $t=0$: $\phi(0)=1$, $T(0)=0$, $DP(0)=0$ and $D(0)=0$, we obtain the probability density for the dwell time between two main steps, $f(t)=\mathrm{d}D/\mathrm{d}t$, as follows

$$f(t)=k_1k_2k_3\left(\frac{e^{-k_1t}}{(k_1-k_2)(k_1-k_3)}+\frac{e^{-k_2t}}{(k_2-k_1)(k_2-k_3)}+\frac{e^{-k_3t}}{(k_3-k_1)(k_3-k_2)}\right), \tag{9}$$

From Eq. (9), the mean dwell time between two main steps is $T_{\mathrm{d}}=1/k_1+1/k_2+1/k_3$, which is rewritten as

$$T_{\mathrm{d}}=\frac{K_{\mathrm{m}}+[\mathrm{ATP}]}{K_{\mathrm{c}}[\mathrm{ATP}]}, \tag{10}$$

where $k_{\mathrm{c}}=k_2k_3/(k_2+k_3)$ and $K_{\mathrm{m}}=k_{\mathrm{c}}/k_{\mathrm{b}}$.

The dwell-time distributions calculated by using Eq. (9) at different ATP concentrations are shown by black solid lines in Fig. 3a, where the three experimentally unavailable parameters are taken as $k_b = 3\times10^7$ $M^{-1}s^{-1}$ [8], $k_2 = 1.64$ s^{-1} and $k_3 = 0.71$ s^{-1} (noting that, by taking $k_2 = 0.71$ s^{-1} and $k_3 = 1.64$ s^{-1}, we have the same results). At low ATP concentrations, i.e., $[ATP] \ll K_m$ or $k_1 = k_b[ATP] \ll k_2, k_3$ (0.02 and 0.2 μM), Eq. (9) becomes $f(t) = k_1 \exp(-k_1 t)$, implying a single-exponential distribution, with the rate $k_1 = k_b[ATP]$ proportional to [ATP] (Fig. 3b; open circles). At intermediate ATP concentrations between 2 and 200 μM, the dwell-time distributions can be approximately fitted by two-exponential functions. At high ATP concentrations, i.e., $[ATP] \gg K_m$ or $k_1 = k_b[ATP] \gg k_2$, k_3 (2000 and 6000 μM), Eq. (9) becomes $f(t) = k_2 k_3 / (k_2 - k_3)[\exp(-k_2 t) - \exp(-k_3 t)]$, implying a two-exponential distribution, with the mean dwell time $T_d = T_{d2} = 1/k_2 + 1/k_3$ independent of ATP concentration. All these results are consistent with the experimental data [8].

5. Rotation rate

From Eqs. (2)–(6), the mean rotation rate of F_1-ATPase is given as

$$V = \frac{1}{3(T_{r1} + T_{r2} + T_{d1} + T_{d2})}, \tag{11a}$$

or, from Eqs.(2)–(4) and(10), it is given as

$$V = \frac{1}{3(T_{r1} + T_{r2} + T_d)}, \tag{11b}$$

where V is in units of revolution per second (r.p.s.) if the rotating times and dwell times are in units of second.

Using Eqs. (11a)–(11b) we calculate the rotation rate under different conditions. The results of rotation rate versus actin length for various ATP concentrations are shown in Fig. 4. It is seen that the theoretical results are consistent with the experimental data [7]. The decrease of the rotation rate with the increase of actin length is due to decrease of the rotating times T_{r1} and T_{r2} (see Fig. 2a), because the dwell times T_{d1} and T_{d2} are independent of the drag friction that is dependent on the actin length. Fig. 5 shows the rotation rate as a function of ATP concentration for a 40-nm bead (corresponding to a small drag friction) and for a 1-μm actin filament (corresponding to large drag friction). For both drag frictions, the dependence of rotation rate on [ATP] fits with Michaelis–Menten kinetics. These results (Fig. 5) are in agreement with the experimental data [8]. In Fig. 6, we show the rotation rate versus drag coefficient for different ATP concentrations. The results are also consistent with the experimental data [8]. From Eqs. (11a)–(11b), it is noted that, at high drag friction, the rotation is limited by the rotating times T_{r1} and T_{r2}; while at low drag friction, the rotation is limited by the dwell times T_{d1} and T_{d2}. The good agreement between all these theoretical results (Figs. 4–6) and experimental data [8] supports the present model.

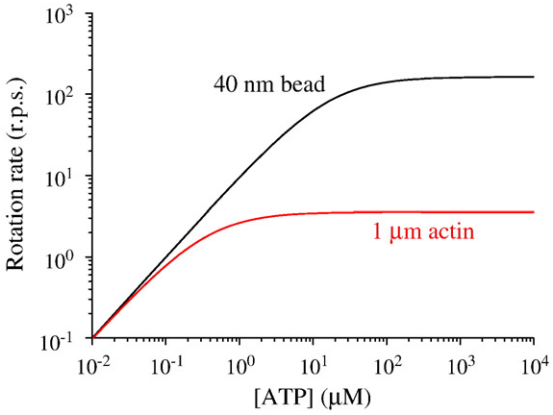

Fig. 5. Rotation rate V versus ATP concentration for a 40-nm bead and for a 1-μm actin filament.

6. Discussion

In the present model, during one ATPase cycle the power stroke results in the eccentric γ-shaft rotated by about 80°and the power stroke occurs upon ATP binding, which gives a free-energy drop of about $14k_BT$. This rotation angle of 80°is determined from Walker's structure [25] and the free-energy drop of about $14k_BT$ delivered by ATP binding is from the kinetic experiments [28,29]. In the kinetic experiments, there are two free-energy drops, with $\Delta G = 14k_BT$ upon ATP binding and $10k_BT$ upon product release. The first drop of $14k_BT$ is attributed to the power stroke driven by ATP binding; while the second drop of $10k_BT$ is attributed to the resumption of the power stroke driven by ADP release. Since the resumption of the power stroke has no contribution to driving the γ-shaft rotation, only $14k_BT$ of the total $24k_BT$ ATP-hydrolysis free energy is delivered directly to turn the γ-shaft.

6.1. The sequential ATPase activities generally follow "bi-site" activation mechanism

In the present model, for the γ-shaft-stimulated ATPase activity, it is assumed that the γ-shaft only stimulates significantly the ATP-binding rate, ATP-hydrolysis rate and Pi-release rate of the β subunit to which it is binding strongly. This is a simpler assumption than that

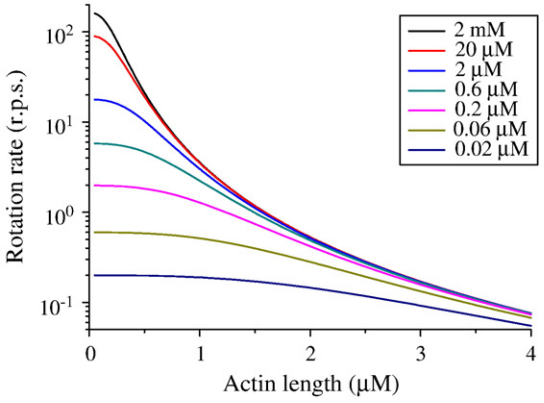

Fig. 4. Rotation rate V versus actin length for various ATP concentrations.

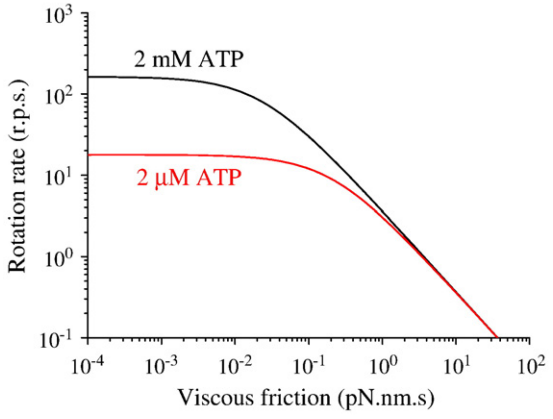

Fig. 6. Rotation rate V versus drag coefficient for different ATP concentrations.

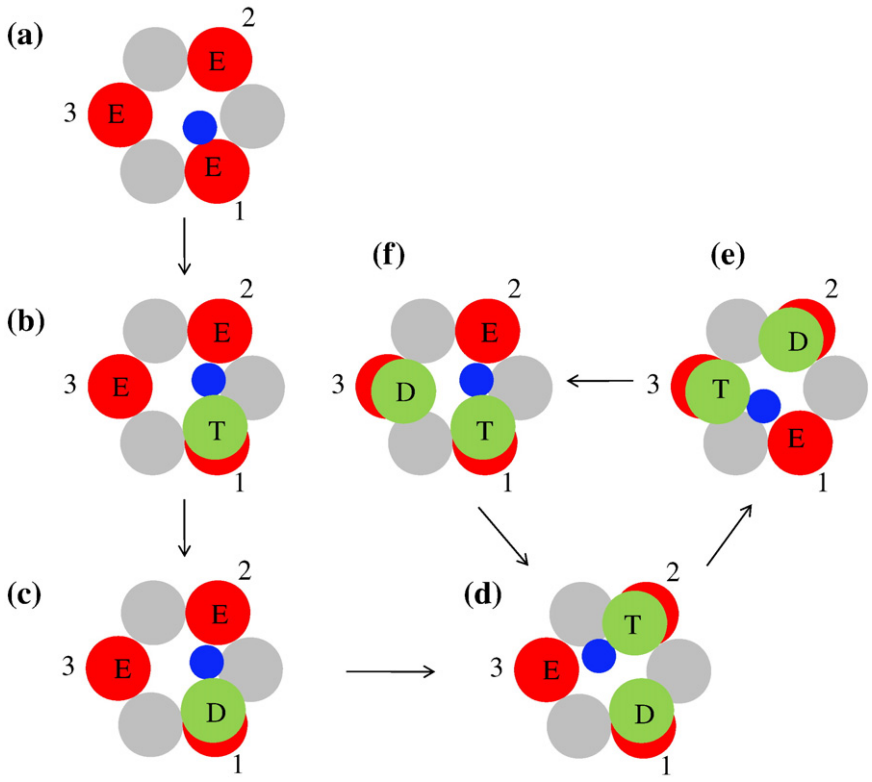

Fig. 7. Schematic illustrations of sequential ATPase activities around the ring (see text for detailed descriptions). The symbols are the same as in Fig. 1.

adopted in the previous model, where γ-shaft not only has significant effects on the ATPase activity of the β subunit to which it is binding strongly but also has significant effects on ATPase activities of other two β subunits [11,13]. Nevertheless, with this simpler kinetic assumption, the present model gives a good explanation to the two-substep rotation and also provides quantitative reproduction of the availably experimental data on the rotating dynamics (Figs. 3–6).

Moreover, this simpler kinetic assumption, together with the asymmetric effect of the power stroke on the γ-shaft, leads automatically to the sequential ATP activities around the ring, as it is generally believed. This is schematically illustrated in Fig. 7. Consider that the three subunits are initially nucleotide free and the γ-shaft binds strongly subunit 1 (Fig. 7a). Stimulated by the strong interaction of the γ-shaft, an ATP binds to subunit 1, inducing the γ-shaft rotated by 80° in the counterclockwise direction (Fig. 7b). After ATP hydrolysis and then Pi release, subunit 1 in ADP state becomes bound weakly to the γ-shaft (Fig. 7c). Since now the γ-shaft is nearer to subunit 2 (40°) than to subunit 3 (200°), it most probably binds subunit 2, which stimulates ATP binding to it (Fig. 7d). Note that, without the stimulation of the γ-shaft, subunit 3 has a very low ATP-binding rate. Now, subunit 2 is in ATP state, subunit 3 is nucleotide free and subunit 1 is in ADP state (Fig. 7d). After ATP hydrolysis and Pi release of subunit 2, the γ-shaft binds subunit 3, which stimulates an ATP bound to it (Fig. 7e). During this period (from Fig. 7c to e), the ADP is most probable to release from subunit 1. Thus, subunit 3 is now bound with ATP, subunit 1 is nucleotide free and subunit 2 is bound with ADP (Fig. 7e). Similarly, after ATP hydrolysis and Pi release of subunit 3, subunit 3 will become ADP state, subunit 1 will become ATP state and subunit 2 will become nucleotide free (Fig. 7f). Then, the states of three subunits will change to those shown in Fig. 7d. Thus, ATPase activities take place sequentially in the counterclockwise direction (Fig. 7d → Fig. 7e → Fig. 7f → Fig. 7d).

From above, we thus see that the sequential ATPase activities generally follow "bi-site" activation mechanism, as proposed by Boyer [33]. However, at very low and very high ATP concentrations, the sequential ATPase activities may not follow this "bi-site" activation mechanism. First, consider the case of very low ATP concentration. An ATP binds to subunit 1 that is binding strongly the γ-shaft (Fig. 8a). After ATP hydrolysis and then Pi release, the γ-shaft is transferred to subunit 2. Now subunit 1 is in ADP state, subunit 2 and subunit 3 are nucleotide free (Fig. 8b). Since it takes a long time for an ATP to bind to subunit 2 due to very low ATP concentration, ADP is most probable to release from subunit 1 and thus all three subunits become nucleotide free (Fig. 8c). Then an ATP binds to subunit 2 that is binding strongly

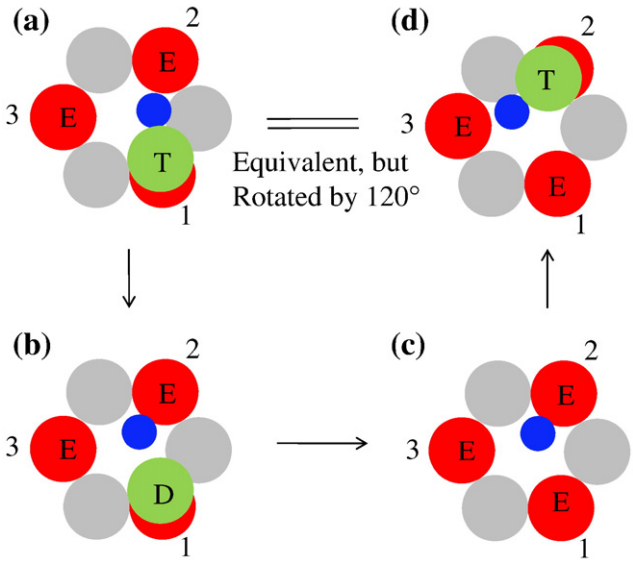

Fig. 8. Schematic illustrations of "uni-site" activation mechanism at very low ATP concentration (see text for detailed descriptions). The symbols are the same as in Fig. 1.

the γ-shaft (Fig. 8d). Fig. 8d is the same as Fig. 8a except that the system is rotated by 120°. Thus, at very low ATP concentration, the sequential ATPase activities may not follow "bi-site" activation mechanism. Second, consider the case of very high ATP concentration. Because of very high ATP-binding rate, after ATP at one subunit is hydrolyzed and then Pi is released, it is possible that the ADP in the next adjacent subunit has not been released. Thus, all three subunits are bound with nucleotide. Therefore, at very high ATP concentration, the sequential ATPase activities may occasionally follow "tri-site" activation mechanism although the main mechanism is still "bi-site" activation.

6.2. Comparison with previous models

In the present model, a 120° rotation consists of two substeps, with the first one of 80° rotation and the second one of 40° rotation. Similar to that proposed in the previous models [11–13,16], the first substep is mainly driven by the driving torque from the ATP-binding-induced power stroke. The second substep (i.e., the passage of the γ-shaft from previous β subunit to next β subunit), which follows the release of Pi, resulted from the free diffusion. This is different from that proposed in the previous models, where the second substep follows the release of ADP and is also driven by the power stroke induced by the ATPase activity. Nevertheless, the results for the mean rotation rates under different values of viscous friction and ATP concentration obtained from the present model (Figs. 4–6) are consistent with those obtained from previous models [11–13,16]. However, some results for the substep and the dwell-time distribution obtained from the present model are different from those inferred from the previous model [13], which is discussed as follows.

In the previous model, it is assumed that the bending motion of the β subunit driven by ATP binding can push against the eccentric γ-shaft rotated by 120°. The pause at $\theta = 0°$ is due to the waiting for ATP binding to subunit 1 (see Fig. 5d in Sun et al. [13]), as in the present model. Some of the free energy induced by the ATP binding in site 1 drives the rotation of the first substep. The pause at $\theta = 80°$ is due to the hindering of subunit 3 bound with ADP. After the ADP in subunit 3 is released, the remaining free energy induced by the ATP binding in site 1 completes the second substep. This is inconsistent with the recent experimental results showed that the second substep follows the release of Pi rather than the release of ADP [26]. Moreover, based on above argument, it can be inferred that, when ATP concentration is very low, ADP bound at site 3 would be released before ATP binding to site 1. This implies that the pause at $\theta = 80°$ would not occur and only pause at $\theta = 0°$ for waiting ATP could occur. Moreover, at high ATP concentration, the pause at $\theta = 0°$ for waiting ATP will not occur and only the pause at $\theta = 80°$ for ADP release will occur. Thus, neither at high nor at very low ATP concentration could the substep be observed. Only at intermediate ATP concentration could the substep be observed and the dwell time at $\theta = 80°$ would be dependent on the ATP concentration. These are inconsistent with the experimental results [8]. In order to avoid the inconsistency between theoretical and experimental results, it was assumed that the ADP-release rate from one site (e.g., site 3) is reduced by 5×10^8 folds when its two adjacent sites (e.g., sites 1 and 2) are nucleotide free [13]. This is a too large reduction! In addition, since the dwell time of pause at $\theta = 80°$ is only determined by the rate of ADP release, it is expected that the dwell-time distribution at high ATP concentration should be fitted with a single exponential. However, the experimental results showed that the distribution is well fitted with two exponentials, implying that two reactions dictate the pause at $\theta = 80°$ [8]. Thus, the theoretical results inferred from the previous model [13] are not consistent with the experimental data.

On the contrary, the dwell time of pause at $\theta = 80°$ in the present model is determined by both the rate of ATP hydrolysis and that of Pi release, which is independent of ATP concentration. The second substep follows the release of Pi. Moreover, the dwell-time distribution has a two-exponential form at high ATP concentration (see Fig. 3). All these are consistent with the experimental results [8,26].

6.3. Comparison with models of hexameric nucleic-acid motor proteins

It is noted that the chemomechanical coupling mechanism of F_1-ATPase presented here is very similar to those proposed for other hexameric nucleic-acid motor proteins such as bacteriophage T7 helicase [34], RuvB [35] and ϕ29 DNA packaging motor (J. Qian et al. unpublished). In the models of those hexameric nucleic-acid motor proteins, the translocation of DNA during one ATPase cycle also consists of two substeps. One substep is driven by power stroke that resulted from the ATP-hydrolysis-induced rotation of the DNA-binding loop. The other substep is the passage of DNA from previous to next adjacent subunits. The high chemomechanical coupling efficiency of those motor proteins is also attained by sequential ATPase activities around the ring induced by the strong interaction of hexameric subunits with DNA.

7. Conclusion

In summary, a physical model for chemomechanical coupling of F_1-ATPase is presented, in which the rotation of γ-shaft during one ATPase cycle consists of two substeps, with one substep of 80° rotation being induced by the power stroke while the other one of 40° rotation being produced from the passage of γ-shaft from previous to next adjacent β subunits. This chemomechanical coupling may be a general mechanism for ring-shaped hexameric motor proteins. Using the model, we analytically studied the dynamics and kinetics of F_1-ATPase. The theoretical results obtained with only three adjustable parameters (k_b, k_2 and k_3) reproduce the available experimental data well.

Acknowledgments

This work was supported by the National Natural Science Foundation of China (Grant Nos. 10834014, 10674173, 30770517) and the National Basic Research Program of China (973 Program) (Grant No. 2009CB930704).

References

[1] P.D. Boyer, The ATP synthase — a splendid molecular machine, Annu. Rev. Biochem. 66 (1997) 717–749.
[2] P.D. Boyer, The binding change mechanism for ATP synthase — some probabilities and possibilities, Biochim. Biophys. Acta 1140 (1993) 215–250.
[3] P.D. Boyer, Catalytic site forms and controls in ATP synthase catalysis, Biochim. Biophys. Acta 1458 (2000) 252–262.
[4] T.M. Duncan, V.V. Bulygin, Y. Zhou, M.L. Hutcheon, R. Cross, Rotation of subunits during catalysis by *Escherichia coli* F1-ATPase, Proc. Natl Acad. Sci. U. S. A. 92 (1995) 10964–10968.
[5] D. Sabbert, S. Engelbrecht, W. Junge, Intersubunit rotation in active F-ATPase, Nature 381 (1996) 623–625.
[6] H. Noji, R. Yasuda, M. Yoshida, K. Kinosita, Direct observation of the rotation of F1-ATPase, Nature 386 (1997) 299–302.
[7] R. Yasuda, H. Noji, K. Kinosita, M. Yoshida, F1-ATPase is a highly efficient molecular motor that rotates with discrete 120° substeps, Cell 93 (1998) 1117–1124.
[8] R. Yasuda, H. Noji, M. Yoshida, K. Kinosita, H. Itoh, Resolution of distinct rotational substeps by submillisecond kinetic analysis of F1-ATPase, Nature 410 (2001) 898–904.
[9] T. Nishizaka, K. Oiwa, H. Noji, S. Kimura, E. Muneyuki, M. Yoshida, K. Kinosita, Chemomechanical coupling in F1-ATPase revealed by simultaneous observation of nucleotide kinetics and rotation, Nat. Struct. Mol. Biol. 11 (2004) 142–148.
[10] H. Ueno, T. Suzuki, K. Kinosita, M. Yoshida, ATP-driven stepwise rotation of F_oF_1-ATP synthase, Proc. Natl. Acad. Sci. U. S. A. 102 (2005) 1333–1338.
[11] H.Y. Wang, G. Oster, Energy transduction in the F_1 motor of ATP synthase, Nature 396 (1998) 279–282.
[12] P. Gaspard, E. Gerritsma, The stochastic chemomechanics of the F_1-ATPase molecular motor, J. Theor. Boil. 247 (2007) 672–686.
[13] S.X. Sun, H.Y. Wang, G. Oster, Asymmetry in the F1-ATPase and its implications for the rotational cycle, Biophys. J. 86 (2004) 1373–1384.
[14] Y. Gao, W. Yang, R.A. Marcus, M. Karplus, A model for the cooperative free energy transduction and kinetics of ATP hydrolusis by F_1-ATPase, Proc. Natl. Acad. Sci. U. S. A. 100 (2003) 11339–11344.

[15] Y. Gao, W. Yang, M. Karplus, A structure-based model for the synthesis and hydrolysis of ATP by F_1-ATPase, Cell 123 (2005) 195–205.
[16] M.S. Liu, B.D. Todd, R.J. Sadus, Kinetics and chemomechanical properties of the F_1-ATPase molecular motor, J. Chem. Phys. 118 (2003) 9890–9898.
[17] M.S. Liu, B.D. Todd, R.J. Sadus, Complex cooperativity of ATP hydrolysis in the F_1-ATPase molecular motor, Biochim. Biophys. Acta 1698 (2004) 197–202.
[18] L. Xu, The coupled chemomechanics of the F_1-ATPase molecular motor, Biochim. Biophys. Acta 1777 (2008) 1422–1431.
[19] J.P. Ma, T.C. Flynn, Q. Cui, G.W. Andrew, L. John, E. Walker, A dynamic analysis of the rotation mechanism for conformational changes in F1-ATPase, Structure 10 (2002) 921–931.
[20] M.M. Hingorani, S.S. Patel, Interactions of bacteriophage T7 DNA primase/helicase protein with single-stranded and double-stranded DNAs, Biochemistry 32 (1993) 12478–12487.
[21] B. Muller, I.R. Tsaneva, S.C. West, Branch migration of Holliday junctions promoted by the *Escherichia coli* RuvA and RuvB proteins: II. Interaction of RuvB with DNA, J. Biol. Chem. 268 (1993) 17185–17189.
[22] Y.R. Chemla, K. Aathavan, J. Michaelis, S. Grimes, P.J. Jardine, D.L. Anderson, C. Bustamante, Mechanism of force generation of a viral DNA packaging motor, Cell 122 (2005) 683–692.
[23] R. Nakamoto, C. Ketchum, M. Al-Shawi, Rotational coupling in the FoF1 ATP synthase, Annu. Rev. Biophys. Biomol. Struct. 28 (1999) 205–234.
[24] R. Nakamoto, C. Ketchum, P. Kuo, Y. Peskova, M. Al-Shawi, Molecular mechanism of rotational catalysis in the F_oF_1 ATP synthase, Biochim. Biophys. Acta 1458 (2000) 289–299.
[25] J. Abrahams, A. Leslie, R. Lutter, J. Walker, Structure at 2.8 Å resolution of F_1-ATPase from bovine heart mitochondria, Nature 370 (1994) 621–628.
[26] K. Adachi, K. Oiwa, T. Nishizaka, S. Furuike, H. Noji, H. Itoh, M. Yoshida, K. Kinosita Jr., Coupling of rotation and catalysis in F1-ATPase revealed by single-molecule imaging and manipulation, Cell 130 (2007) 309–321.
[27] H. Sielaff, H. Rennekamp, S. Engelbrecht, W. Junge, Functional halt positions of rotary F_OF_1-ATPase correlated with crystal structures, Biophys. J. 95 (2008) 4979–4987.
[28] M. Al-Shawi, D. Parsonage, A. Senior, Kinetic characterization of the unisite catalytic of seven β-subunit mutant of F_1-ATPase from *Escherichia coli*, J. Biol. Chem. 264 (1989) 15376–15383.
[29] J. Weber, A. Senior, Catalytic mechanisms of F1-ATPase, Biochim. Biophys. Acta 1319 (1997) 19–58.
[30] K. Kinosita, R. Yasuda, H. Noji, K. Adachi, A rotary molecular motor that can work at near 100% efficiency, Philos. Trans. Biol. Sci. 355 (2000) 473–490.
[31] O. Panke, D.A. Cherepanov, K. Gumbiowski, S. Engelbrecht, W. Junge, Viscoelastic dynamics of actin filaments coupled to rotary F-ATPase angular torque profile of the enzyme, Biophys. J. 81 (2001) 1220–1233.
[32] P. Xie, S.-X. Dou, P.-Y. Wang, Mechanism for unidirectional movement of kinesin, Chin. Phys. 14 (2005) 734–743.
[33] P.D. Boyer, Catalytic site occupancy during ATP synthase catalysis, FEBS Lett. 512 (2002) 29–32.
[34] P. Xie, On translocation mechanism of ring-shaped helicase along single-stranded DNA, Biochim. Biophys. Acta 1774 (2007) 737–748.
[35] P. Xie, Model for RuvAB-mediated branch migration of Holliday junctions, J. Theor. Biol. 249 (2007) 566–573.